Am J Cancer Res 2023;13(3):835-851
www.ajcr.us /ISSN:2156-6976/ajcr0148692

*Original Article*

# The mechanism of long-chain acyl-CoA synthetase 3 in inhibiting cell proliferation, migration, and invasion in clear cell renal cell carcinoma

Lin Zhang[1], Bo Wu[2], Dongwen Wang[1,3]

*[1]Shanxi Medical University, Taiyuan 030001, Shanxi, P. R. China; [2]Department of Urology, First Hospital of Shanxi Medical University, Taiyuan 030001, Shanxi, P. R. China; [3]National Cancer Center/National Clinical Research Center for Cancer/Cancer Hospital & Shenzhen Hospital, Chinese Academy of Medical Sciences and Peking Union Medical College, Shenzhen 518116, Guangdong, P. R. China*

Received December 22, 2022; Accepted March 6, 2023; Epub March 15, 2023; Published March 30, 2023

**Abstract:** Long-chain acyl-CoA synthases 3 (ACSL3) can activate long-chain fatty acids, which are often deregulated in tumors. However, the biological function of ACSL3 in clear cell renal cell carcinoma (ccRCC) is still unclear. In this research, the expression level, prognostic value, GO and KEGG functional enrichment analyses, genomic changes, clinical significance, immune infiltration of ACSL3 in ccRCC were comprehensively analysed. The expression levels of ACSL3 in ccRCC tissues were detected by quantitative reverse transcription-polymerase chain reaction (RT-qPCR), immunohistochemical staining (IHC), and Western blotting analysis. The proliferation, invasion, migration, apoptotic and lipid synthesis abilities of ccRCC cells were assessed using the cell counting kit (CCK-8), clone formation, scratch assay, Transwell assay, flow cytometry and Oil Red O assay, respectively. The results showed that ACSL3 was obviously downregulated in ccRCC and significantly associated with poor prognosis and clinicopathological factors of ccRCC patients. Additionally, the functional enrichment analysis indicated that ACSL3 was mainly involved in lipid synthesis and metabolism. The result of immune infiltration analysis proved that ACSL3 might regulate the tumor microenvironment of ccRCC. In addition, we demonstrated that overexpression of the ACSL3 could inhibit the proliferation, migration, and invasion of ccRCC cells, and promote apoptosis, reduce abnormal lipid accumulation. In conclusion, ACSL3 might be a novel ccRCC biomarker and the target for ccRCC tumor therapy.

**Keywords:** ACSL3, clear cell renal cell carcinoma, prognosis, tumor microenvironment, biomarker

## Introduction

Cancer is a major public health problem worldwide and results in death in humans [1]. Clear cell renal cell carcinoma (ccRCC) is a malignant tumor caused by renal tubular epithelial cell lesions and accounts for about 2% of the world's human malignancies and 80%-90% of renal malignancies in adults [2]. The occurrence and development of ccRCC can be influenced by several factors, such as smoking, obesity, occupation, underlying diseases, drinking, and familial genetic inheritance [3]. Although the diagnosis and treatment of ccRCC have improved over the past two decades, it is often detected at a late stage with a poor prognosis [4]. Hence, early detection is critical to reducing mortality. However, there is no specific biomarker for ccRCC. Thus, the identification of reliable prognostic markers and therapeutic targets is vital for the treatment of ccRCC.

Metabolism is the basis of all biological activities. Metabolic disorders exist in tumors, and cancer cells are reprogrammed to meet their needs for energy consumption, stress tolerance, proliferation, and microenvironmental changes [5]. An increasing number of studies have shown the presence of lipid metabolism disorders in ccRCC [6]. Compared with normal renal tissues, fatty acid oxidation (FAO) is decreased, and enzymes involved in fat storage are increased in ccRCC [7-9]. Also, there is an abnormal accumulation of cholesteryl esters and long-chain fatty acids in ccRCC tissues, which provides nutritional raw materials for the

proliferation and metastasis of tumor cells. Existing studies have reported that metabolic disorders in ccRCC cells are regulated by a variety of oncogenes or oncogenic pathways, such as the myeloma proto-oncogene (MYC), P53, hypoxia-inducible factor-1a and 2a (HIF-1a and HIF-2a), adenosine 5'-monophosphate-activated protein kinase (AMPK)/mTOR signaling pathway, and the PI3K/Akt signaling pathway [10]. Abnormal lipid metabolism in ccRCC may affect cellular function; however, the molecular mechanism regulating the tumorigenesis of ccRCC remains unclear.

Long-chain acyl-CoA synthetases (ACSLs) can activate 12-20-carbon long-chain fatty acids that must be activated in vivo to participate in metabolic pathways. Five family members of ACSLs were found in mammals, namely, ACSL1, ACSL3, ACSL4, ACSL5, and ACSL6 [11, 12]. The long-chain acyl-CoA synthetase 3 (ACSL3) gene is located on human chromosome 2, and its encoded isoenzyme preferentially activates palmitic acid and catalyzes the synthesis of fatty acyl-CoA esters [13]. ACSL3 is abundant in the human brain and prostate, mainly in the endoplasmic reticulum, mitochondria, and lipid droplets of cells [14], and the N-terminal structural domain of ACSL3 regulates lipid droplet position and fatty acid uptake. The abnormal expression of ACSL3 has been shown to play an important role in the development and progression of various tumors [15]. For example, the overexpression of ACSL3 is associated with worse clinical outcomes in patients with high-grade non-small cell lung cancer (NSCLC) [16]. Besides, the ACSL3-LPIAT1 signaling axis can drive prostaglandin synthesis in NSCLC and has potential therapeutic value [17]. ACSL3 promotes steroidogenesis in prostate cancer and is associated with poor prognosis [18]. ACSL3 is also strongly associated with human fibrosarcoma, leiomyosarcoma, rhabdomyosarcoma [19], breast cancer [20], and melanoma [21]. The ACSL3-PAI-1 signaling axis can also promote the progression of pancreatic cancer by mediating tumor-stromal crosstalk [22]. However, the biological role of ACSL3 in ccRCC remains unclear.

In this study, the expression level, prognostic value, and mutation type of ACSL3 in ccRCC were analyzed by the cancer genome atlas (TCGA) dataset and several online packages for bioinformatics analysis. The expression levels of the ACSL3 in ccRCC tissues and cells were verified experimentally. Cell transfection experiments were used to investigate the effect of ACSL3 expression on the biological function of ccRCC cells. The results revealed the potential application of ACSL3 as a prognostic marker for ccRCC, providing a research basis for the diagnosis and treatment of ccRCC.

## Materials and methods

### *Clinical sample collection and ethics approval*

In this study, ccRCC and adjacent noncancerous tissues surgically removed at the Urology Department of the First Hospital of Shanxi Medical University from October 2021 to October 2022 were selected as the study subjects. All included subjects had complete clinical and pathological data, and the tumor tissues were pathologically diagnosed as ccRCC without lesions in the adjacent noncancerous tissues. Tumor tissues and adjacent normal tissues (more than 2 cm away from the tumor margin) were excised from the patients by surgical resection. Some tissues were fixed in 10% formalin, and the remaining were immediately stored in liquid nitrogen until further analysis. This study was reviewed and approved by the Medical Ethics Committee of the First Hospital of Shanxi Medical University, and a signed written informed consent according to the Declaration of Helsinki was obtained from patients participating in this study.

### *Acquisition and processing of data on ACSL3 gene expression level and their prognostic value*

The online bioinformatics analysis website UALCAN (http://ualcan.path.uab.edu/index.html) was used to analyze the RNA sequencing data of ccRCC and adjacent normal tissues from the TCGA database. These data were used to analyze the expression levels of the ACSL3 in ccRCC (533 samples) and normal tissues (72 samples). The expression data of the ACSL3 gene in ccRCC samples were downloaded from the TCGA database; samples with an expression level of 0 and follow-up time shorter than 30 days were filtered, and log2 (x+0.001) transformation was performed for each expression value. The best cut-off value of ACSL3 was calculated using the maxstat package of the sta-

tistical software R (Maximally selected rank statistics with several *P*-value approximations version: 0.7-25). Based on the best cut-off value, patients were divided into ACSL3 upregulated and downregulated groups, and the prognostic differences between the two groups were further analyzed using the "survfit" package of R software. The correlation of ACSL3 expression with overall survival (OS), disease-specific survival (DSS), and progression-free interval (PFI) in ccRCC tumors were analyzed, and the significance of prognostic differences between different groups of samples was assessed using the Log-rank test.

*Protein level analysis*

The Human Protein Atlas database (HPA: https://www.proteinatlas.org/) was used to investigate the protein expression levels of ACSL3 in ccRCC tissues. Moreover, the GeneCards online tool (https://www.genecards.org/) was used to visualize the subcellular location of ACSL3.

*ACSL3-related gene enrichment analysis*

The online database STRING (https://string-db.org/) was used to construct a protein-protein interaction network for ACSL3. Based on the STRING database, we obtained 50 ACSL3-binding proteins supported by experimental evidence. The top 100 genes associated with ACSL3 expression were obtained using the GEPIA2 database (http://gepia2.cancer-pku.cn/#index). Then, we combined the genes of these two datasets for the KEGG pathway, GO biological process (BP), cellular constituent (CC), and molecular function (MF) functional enrichment analysis. Gene lists were uploaded to the DAVID database for annotation and visualization. The gene enrichment results were visualized using the "tidyr" and "ggplot2" packages in R software. *P*-values of $< 0.05$ were considered statistically significant.

*Genetic alteration analysis data and ACSL3 expression in different clinical subgroups of ccRCC*

The c-BioPortal database (https://www.cbioportal.org/) is a cancer genomics database, which was used to study genomic alterations of ACSL3 in ccRCC, such as mutation frequency, mutation types, and copy number alteration (CNA), as well as mutation site information. The "mutations" module was used to obtain a schematic representation of the ACSL3 protein structure and display its mutation sites. The relationship between the ACSL3 expression and the clinicopathological features of ccRCC was analyzed using the UALCAN database.

*Assessment of ACSL3 expression in single-cell RNA-seq datasets*

The tumor immunological single-cell center (TISCH, http://tisch.compgenomics.org/home/) is a database for the tumor microenvironment (TME), with scRNA-seq datasets that provide detailed cell-type annotations at the single-cell level. The TISCH database was used to search for the ACSL3 gene, and the cell-type annotations were selected for the study of "major cell lines". Moreover, the colocalization of ACSL3 with the KIRC single-cell datasets GSE111360, GSE139555, GSE145281_aPDL1, GSE121636, GSE159115, as well as GSE171306, was analyzed.

*Cell culture and transfection*

The ccRCC cell lines ACHN, 769P, 786O, renal cell line 293T, cell basic culture medium minimum essential medium (MEM), and 1640 culture medium were purchased from Procell (Wuhan, China). Fetal bovine serum (FBS) was purchased from Gibco (Gibco, Grand Island, NY, USA), streptomycin, penicillin sodium, and trypsin were purchased from Solarbio (Solarbio, Beijing, China), while lipo3000 was purchased from Thermo Fisher (Thermo Fisher Scientific, Waltham, USA). ACSL3 overexpression plasmid h-ACSL3 and null plasmid pcDNA3.1-3xflag for transfection were purchased from Hanheng (Hanbio, Shanghai, China). The ccRCC cell line ACHN was cultured in the MEM cell culture medium supplemented with 10% FBS, 1% streptomycin, and 1% penicillin sodium, which was named cell complete culture medium, while 769P, 786O, and 293T cells were cultured in the 1640 cell culture medium supplemented with 10% FBS, 1% streptomycin, and 1% penicillin sodium at 37°C in a 5% $CO_2$ incubator until the logarithmic growth phase was reached. Cells were digested using trypsin and sub-cultured 1:3 when they grew to a fusion of 70% to 90%. The cell culture medium was exchanged after 48 h-72 h of cell growth. For

cell transfection, cells were inoculated into six-well plates, and when the cell density reached 60% to 70%, the ACSL3 overexpression plasmid h-ACSL3 and empty plasmid pcDNA3.1-3xflag were transfected using the lipo3000 transfection reagent, according to the manufacturer's instructions. Cells were cultured at 37°C in a 5% $CO_2$ incubator after adding the transfection reagent. After 6 h of transfection, the culture medium was exchanged with the new cell culture medium supplemented with 10% FBS. Subsequent experiments were performed 48 h after transfection.

*Quantitative reverse transcription-polymerase chain reaction*

ACSL3 mRNA expression was detected in 60 pairs of ccRCC tissues and adjacent non-cancerous tissues. TRIzol reagent, mRNA reverse transcription kit TransScript® Uni All-in-One First-Strand cDNA Synthesis SuperMix for qPCR (one-step gDNA removal), and qPCR kit PerfectStart Green qPCR SuperMix were purchased from TransGen Biotech (Beijing, China). Cell samples were lysed with TRIzol reagent, and the total RNA from tissues and cells was extracted according to the manufacturer's instructions. Extracted RNA was reverse transcribed into cDNA according to the TransScript® Reverse Transcription Kit instructions, and the resultant cDNA was subjected to qPCR using the PerfectStart Green qPCR SuperMix kit. Using GAPDH as an internal reference, the relative expression levels of ACSL3 mRNA and DAPDH were calculated using the $2^{-\Delta\Delta Ct}$ method. Primer sequences used for quantitative reverse transcription-polymerase chain reaction (RT-qPCR) were: ACSL3 forward primer, 5'-GCCGAGTGGATGATAGCTGC-3'; ACSL3 reverse primer, 5'-ATGGCTGGACCTCCTAGAGTG-3'; GAPDH forward primer, 5'-GCTCTCTGCTCCTCCTGTTC-3'; GAPDH reverse primer, 5'-ACGACCAAATCCGTTGACTC-3'.

*Immunohistochemical staining*

Immunohistochemistry (IHC) was used to detect the protein expression levels of ACSL3 in 30 pairs of ccRCC tissues and adjacent normal tissues. Pathological tissue sections were obtained from patients with pathologically confirmed ccRCC, which were then deparaffinized, hydrated, and endogenous peroxidase was removed with hydrogen peroxide to repair tissue antigens. Then, the sections were washed thrice with PBS for 2 min each, incubated with the anti-ACSL3 antibody (1:100, Abclonal, USA) in an incubator at 37°C for 1 h, and cooled at room temperature for 30 min. The sections were then rinsed with PBS, after which secondary antibodies (Boster, China) were added and incubated for 20 min. After rinsing with PBS, color development was performed using the DAB kit (Boster, China), which was then terminated by microscopic observation. Subsequently, hematoxylin was used to counterstain acidophilic structures, which were turned blue, after which the section was dehydrated. Then they were made transparent, and mounted with neutral resin. Finally, the stained sections were read by pathologists.

*Western blot analysis*

The total protein was extracted from the cells or tissues after 48 h of transfection using the RIPA reagent (Boster, China), and the protein concentrations were quantified using a BCA kit (Boster, China). Then, the protein-loading buffer (Boster, China) and RIPA reagent were added to dilute the protein samples to the same concentration, and the samples were boiled at 100°C for 5 min in a water bath to denature the protein. The protein samples were stored at -20°C. Then, the proteins were separated by SDS-PAGE (Meilunbio, China) and transferred onto PVDF membranes (Boster, China). The PVDF membranes were blocked using 5% skimmed milk powder for 2 h and incubated overnight at 4°C with anti-ACSL3 antibody (1:1000, Abclonal, USA) or anti-GAPDH antibody (1:1000, Boster, China). The membrane was washed four times with TBST for 5 min each time, followed by incubation with the secondary antibody (1:3000, Boster, China) at room temperature for 1 h. Then, the membrane was washed four times with TBST for 5 min each time again, and finally, the signal was visualized with an enhanced chemiluminescence kit (Buster, China) and analyzed using the Image J software.

*Cell counting kit-8 assay*

Cells were digested with trypsin and seeded into 96-well plates at a density of $3 \times 10^3$ cells/100 μL/well, with five duplicate wells set up for each group, and incubated at 37°C in a 5% $CO_2$ incubator. The cells were then treated with CCK-8 reagent after 0 h, 24 h, 48 h, 72 h,

and 96 h, respectively. The cell culture medium was removed, and then 100 μL of fresh basal culture medium and 10 μL of CCK-8 reagent (Boster, California, USA) were added to each well, and the cells were incubated at 37°C in a 5% $CO_2$ incubator for 1.5 h in the dark. Finally, the absorbance of the 96-well plates at 450 nm was determined using a microplate reader.

*Clone formation assay*

The cells were digested with trypsin to prepare cell suspensions, seeded in 6-well plates at a density of 1000 cells/well, shaken uniformly, and incubated at 37°C in a 5% $CO_2$ incubator. The cell complete culture medium was exchanged with new medium every three days to observe cell growth, and the culture was stopped when 50-200 cell colonies were formed. Then, they were fixed with 4% paraformaldehyde for 20 min, washed thrice times with PBS, stained with 0.1% crystal violet staining solution for 10 min, and the number of cell colonies was counted under a microscope and photographed using a camera.

*Wound healing test*

After cells in h-ACSL3 group and control group were observed to cover the 6-well plates, the bottom of the plate was scratched perpendicularly with sterile 200 μL tips, and cell debris was washed off with PBS for 3 times. Then, the basal medium without FBS was added to culture cells. Each group was photographed using a microscope after 0 h, 12 h, 24 h, and 48 h of cell growth. Scratch-healing areas were measured using the ImageJ software.

*Transwell migration and invasion assay*

Cells were digested with trypsin, neutralized with culture medium without FBS, after centrifugation, they were resuspended to prepare cell suspensions. The density of the cell suspension was adjusted to $3 \times 10^5$ cells/mL and 200 μL of cell suspension was added to the upper chambers (Corning, USA) paved with or without Matrigel. The chambers were placed in 24-well plates, to which 600 μL of culture medium containing 20% FBS was added and incubated at 37°C in a 5% $CO_2$ incubator. After 24 h of incubation, the culture was stopped, the cells of the upper chambers were wiped off with a cotton swab, washed with PBS, fixed in 4% paraformaldehyde for 20 min, stained with crystal violet staining solution for 10 min, and photographed using a microscope. The number of the cells were calculated by ImageJ software.

*Flow cytometry assays for cell apoptosis*

The cells were digested with EDTA-free trypsin, after centrifugation, they were washed twice with PBS, centrifuged again to collect the cells, and the cell suspension was prepared using the binding buffer from the kit. Then, 100 μL of the cell suspension was transferred to a 1.5 mL centrifuge tube to make the total number of cells no less than $1 \times 10^5$, after which Annexin V-FITC and PI staining solutions (Meilunbio Company, Dalian, China) were added. Single-stain sets were also prepared to adjust the flow cytometry parameters. The centrifuge tubes were then incubated at room temperature in the dark for 15 min. After that, 400 μL of the binding buffer working solution was added to each tube, mixed well gently, and analyzed using a flow cytometer.

*Oil Red O staining*

Cells were cultured in 6-well plates, and the culture medium was changed 48 h after cell transfection. The cells were washed twice with PBS, after which 4% paraformaldehyde was added to fix the cells for 20 min. The cells were then washed twice with distilled water and soaked in 60% isopropanol for 30 s. Then, the cells were stained with freshly prepared Oil Red O staining solution for 20 min and soaked again in 60% isopropanol for 30 s. Next, the cells were washed with distilled water five times until all excess stain was washed off. Finally, Mayer's hematoxylin violet staining solution was added to counterstain the nucleus for 2 min. The excess stain was then discarded, and the cells were dipped in distilled water 2-5 times. The cells were covered with 1 mL of distilled water, and observed using a microscope.

*Statistical analysis*

The statistical software SPSS 26.0 and GraphPad Prism 9.3 were used for the analysis. All experiments were performed in triplicate. The measurement data conforming to normal distribution were expressed as means ± standard deviation (M ± SD), and an independent samples t-test was used to compare the two

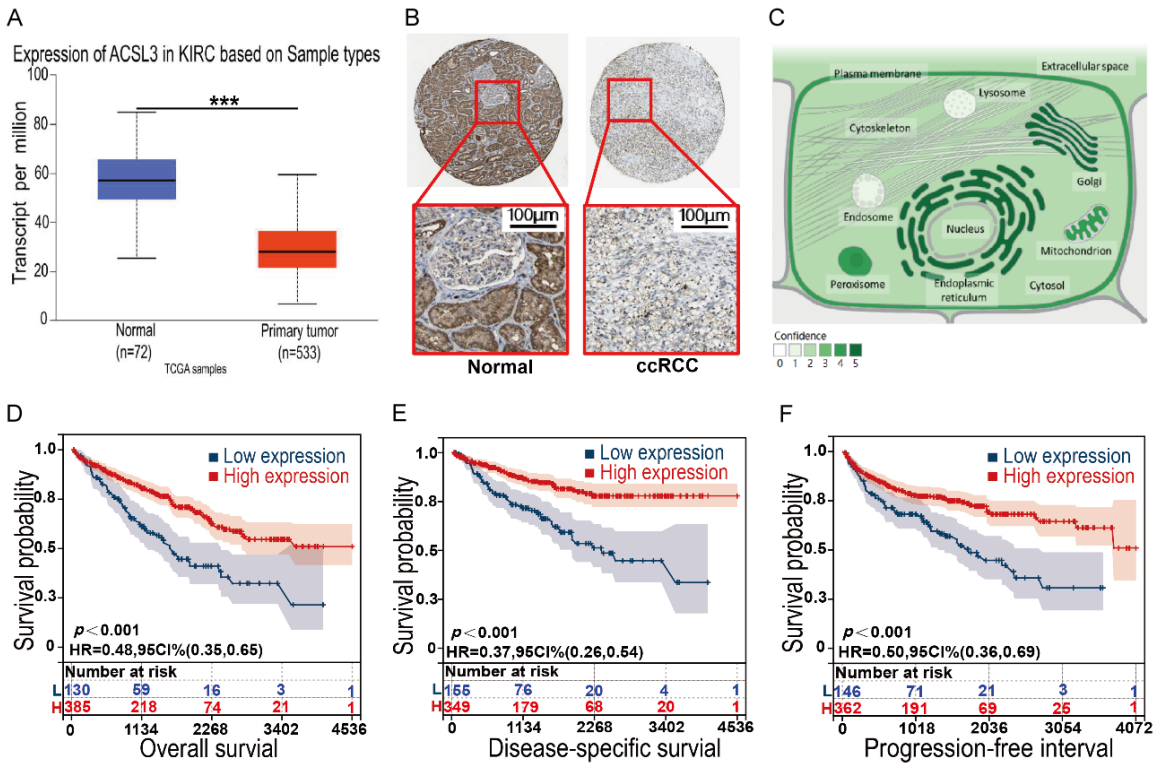


**Figure 1.** The expression level, cellular localization, and survival prognosis of ACSL3 in ccRCC. A. The mRNA expression levels of ACSL3 in ccRCC tissues from the TCGA datasets. B. The protein expression levels of ACSL3 in ccRCC and normal renal tissues from the HPA database. C. The subcellular localization of ACSL3 expression in cells. D-F. Prognostic analysis of ACSL3 in ccRCC based on Kaplan-Meier analysis. D. The correlation between ACSL3 expression and OS. E. The correlation between ACSL3 expression and DSS. F. The correlation between ACSL3 expression and PFI. OS, overall survival; DSS, disease-specific survival; DFS, disease-free interval; PFI, progression-free interval. *ns*, no statistical significance; $^{*}P < 0.05$; $^{**}P < 0.01$; $^{***}P < 0.001$; $^{****}P < 0.0001$.

groups. One-way analysis of variance was used for comparisons of multiple groups. *P*-values of < 0.05 were considered statistically significant.

## Results

### *The expression level and prognostic value of ACSL3 in ccRCC*

In this study, after analyzing the TCGA database using the UALCAN bioinformatics website, it was observed that ACSL3 gene was significantly downregulated in ccRCC tissues than in normal renal tissue (**Figure 1A**). IHC of the HPA database revealed that the ACSL3 protein was expressed in normal renal tubules and decreased in ccRCC tissues (**Figure 1B**). The GeneCards database revealed the subcellular localization of ACSL3 protein, which was mainly expressed on the Golgi apparatus, endoplasmic reticulum, peroxisomes, mitochondria, and plasma membrane (**Figure 1C**). Kaplan-Meier survival analysis revealed that ACSL3 downregulation was associated with poorer OS, DSS, and PFI in ccRCC patients (**Figure 1D-F**).

### *Molecular interaction network and enrichment analysis*

To gain insight into the possible role of ACSL3 in tumorigenesis, we analyzed molecules interacting with ACSL3 using STRING and GEPIA2 websites. Based on the STRING analysis, we obtained 50 ACSL3-binding genes, the interaction network of which is presented in **Figure 2A**. The top 100 genes associated with ACSL3 expression were obtained using the GEPIA2 website in combination with all tumor expression data from TCGA.

The intersection of the top 50 ACSL3-binding genes with the top 100 most ACSL3-relevant genes was analyzed to obtain one common

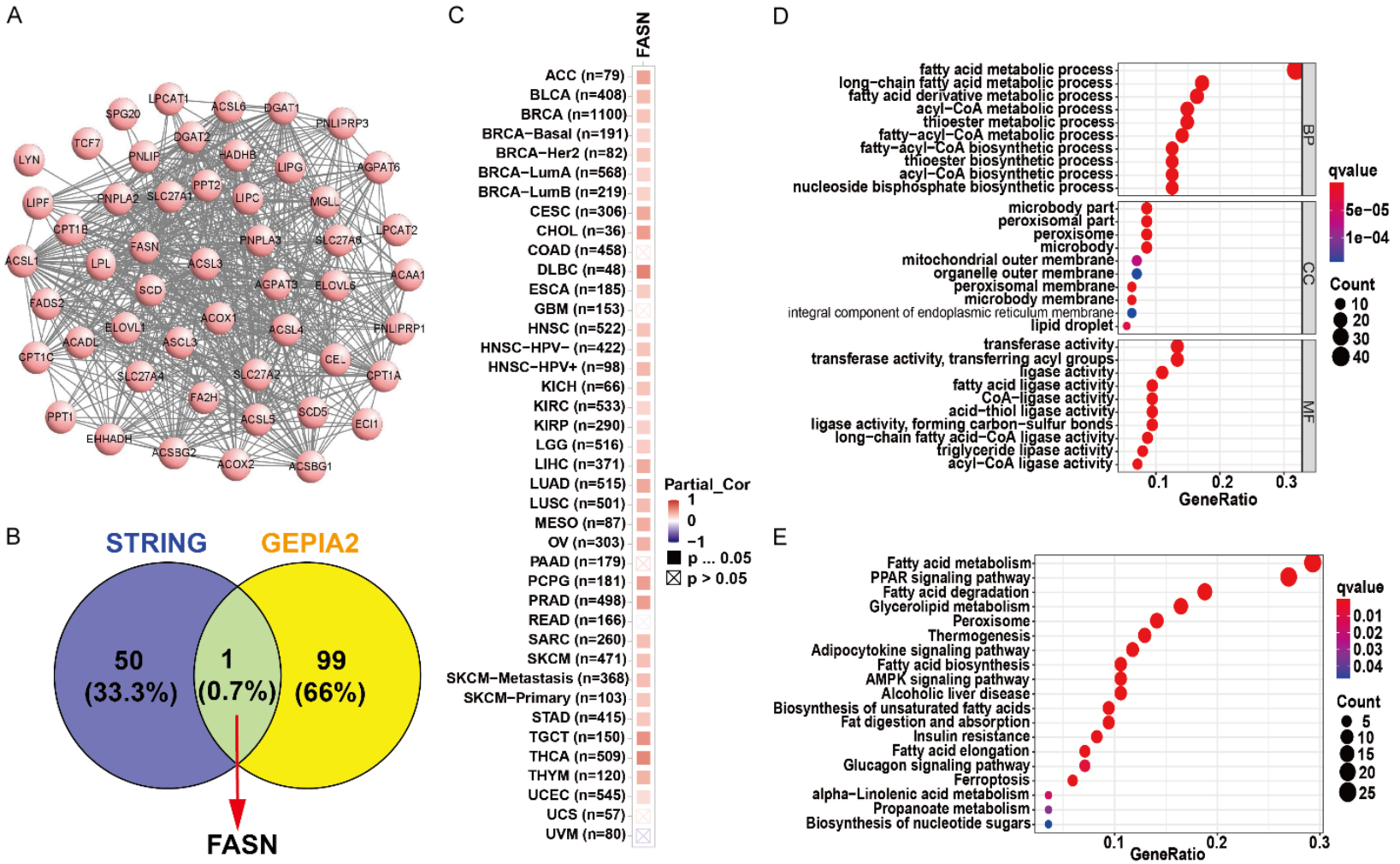


**Figure 2.** Molecular interaction network and functional enrichment analysis of ACSL3-related genes. A. The binding proteins of ACSL3 by the STRING website. B. Overlapping sections show that FASN is the common gene in STRING and GEPIA2 datasets. C. The FASN gene and ACSL3 gene are positively associated with various tumors. D. GO (CC, MF, BP) functional enrichment analysis of the molecules interacting with ACSL3. E. KEGG functional enrichment analysis of the molecules interacting with ACSL3. *ns*, no statistical significance; $^{*}P < 0.05$; $^{**}P < 0.01$; $^{***}P < 0.001$; $^{****}P < 0.0001$.

gene, FASN (**Figure 2B**). FASN is a well-studied gene that plays an important role in tumor metabolism, and the expression level of ACSL3 was positively correlated with the expression of the FASN gene in most cancer types (**Figure 2C**). GO and KEGG functional enrichment analysis of genes from both sets of data indicated that these genes were most significantly related to lipid metabolism, long-chain fatty acid metabolism, lipid synthesis, and the PPAR-signaling pathway (**Figure 2D**, **2E**).

*Genetic and expression alterations of the ACSL3 gene in different clinical subgroups of ccRCC*

The cBioPortal website was used to analyze the genomic alterations of the ACSL3 gene in ccRCC. The results indicated that genomic mutations in ACSL3 occurred in 1.7% of the ccRCC patients (**Figure 3A**). There are multiple mutation types of ACSL3 in ccRCC, including deep deletion, shallow deletion, diploid, and gain (**Figure 3B**). Among them, the main mutation type was "mutation", followed by "amplification" (**Figure 3C**). Moreover, the ACSL3 mutation site and the protein 3D structure were obtained (**Figure 3D**, **3E**). Next, the UALCAN database was used to explore the expression level of ACSL3 in different clinical features of ccRCC. It was observed that ACSL3 was significantly correlated with different tumor grades and stages, as well as the age, nodal metastasis status, subtype, gender, and race of ccRCC patients (**Figure 3F-L**). The above results suggest that the ACSL3 gene undergoes genomic alterations and differential expression in tumor tissues and is significantly correlated with the different clinicopathological features of ccRCC, suggesting that ACSL3 plays an important role in the development of ccRCC.

*The single-cell localization of ACSL3 in KIRC*

We analyzed cell types at the single-cell level and focused on the TME of ccRCC to analyze the correlation between ACSL3 expression and immune abundance (**Figure 4A-F**). We found that the colocalization of ACSL3 in various types of cells was primarily involved in immune regulation in KIRC datasets, which are GSE111360, GSE139555, GSE121636, GSE159115, and GSE171306, as well as in metastatic and PDL1 immunotherapeutic datasets GSE145281aPDL1. Moreover, we observed that ACSL3 was mainly distributed in monocytes and macrophages (mono/macro), CD8 T cells, mast cells, and NK cells in the GSE111360, GSE139555, GSE121636, GSE159115, and GSE171306 datasets (**Figure 4G-K**). Furthermore, ACSL3 was mainly distributed in the mast cells, CD4T conv cells, NK cells, and B cells, and the least in T proliferation cells in GSE145281_aPDL1 data (**Figure 4L**). Overall, ACSL3 was associated with the abundance of multiple immune cells in ccRCC and may mediate the malignant phenotype of tumors by regulating the microenvironment.

*ACSL3 expression is downregulated in ccRCC tissues*

The mRNA and protein expression levels of ACSL3 in ccRCC tissues and adjacent normal tissues were determined by RT-qPCR, Western blot, and IHC staining analysis. RT-qPCR was performed on 60 cases of ccRCC and adjacent tissues. The RT-qPCR result indicated that the mRNA expression of ACSL3 was significantly lower in ccRCC tissues than in normal renal tissues, which was consistent with the results of TCGA (**Figure 5A**). Western blot analysis indicated that the ACSL3 protein expression level was lower in ccRCC tissues than paired adjacent noncancerous tissues (**Figure 5B**, **5C**). IHC was used to detect the expression of ACSL3 in 30 cases of ccRCC tissues, and the expression level of ACSL3 in ccRCC was quantitatively analyzed by the mean density. The results showed that the mean density of ACSL3 IHC staining in ccRCC tissues was lower than that in adjacent normal tissues (**Figure 5D**, **5E**).

*ACSL3 overexpression inhibits the proliferation of cancer cells*

The mRNA and protein expression levels of ACSL3 in ccRCC cell lines (ACHN, 769P, 786O) and normal renal cells (293T) were also examined using RT-qPCR and Western blot analysis. The results showed that the expression level of ACSL3 was significantly lower in ccRCC cell lines than that in 293T cell (**Figure 6A**, **6B**). Among the three ccRCC cell lines, the expression level of ACSL3 was the least in ACHN cells. Therefore, ACHN was selected for the subsequent experiments. Firstly, we obtained h-ACSL3 cells and control cells by transfection. RT-qPCR and Western blot were used to demonstrate the higher expression level of ACSL3

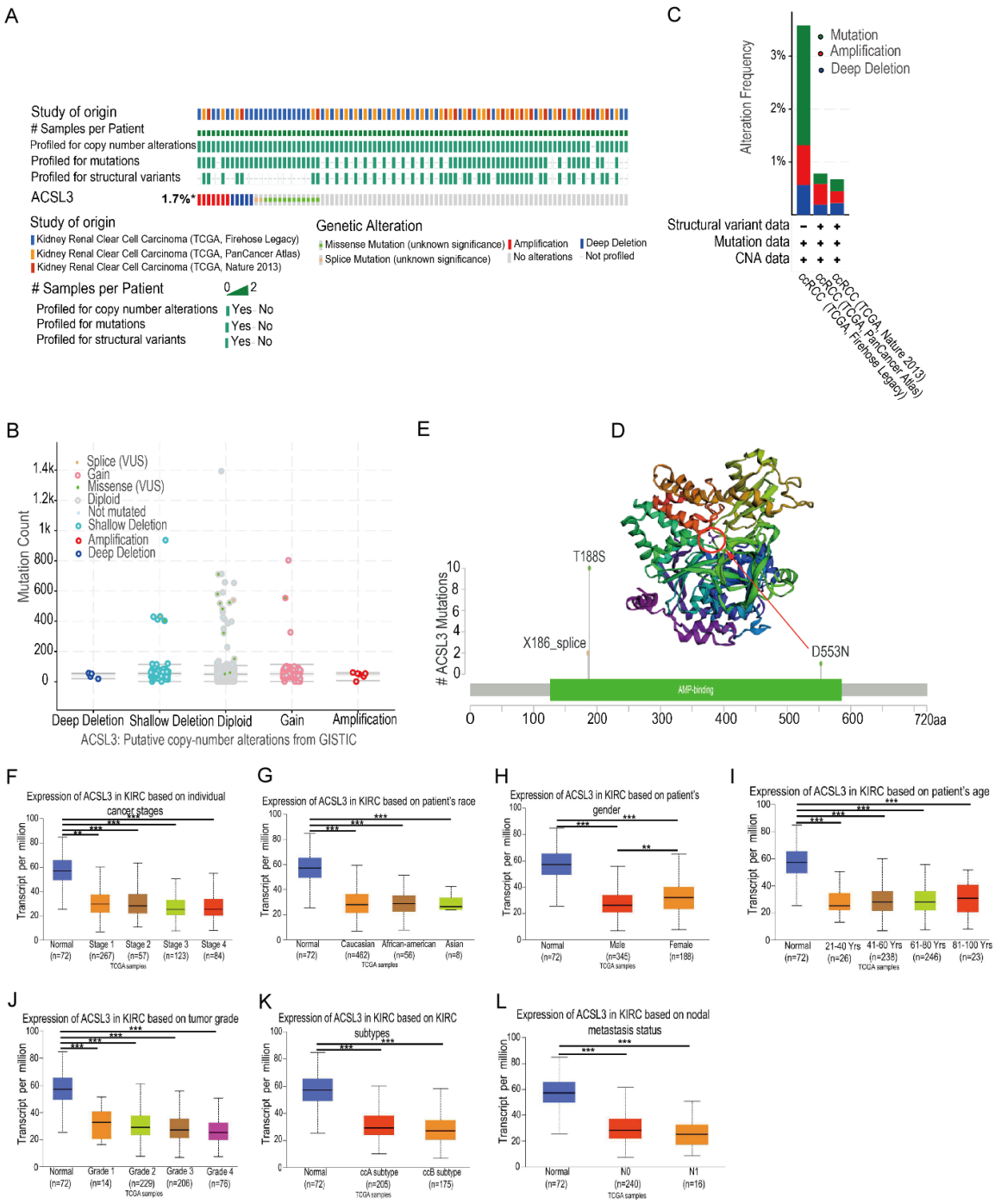


**Figure 3.** (A-E) Genomic alterations of ACSL3 in ccRCC analyzed by the cBioPortal database and (F-L) the differential expression of ACSL3 in ccRCC with different clinical subgroups analyzed by the UALCAN database. (A) OncoPrint of ACSL3 gene alterations in the ccRCC cohort. Different colors represent different types of genetic alterations, and amplification accounted for the largest proportion. (B) The main type of ACSL3 gene alterations in ccRCC groups. (C) The mutation and CNA status of ACSL3 in ccRCC using the cBioportal database. (D) The three-dimensional structure of the ACSL3 protein and the mutation site (D553N) was displayed in the 3D structure of ACSL3. (E) The mutation sites of ACSL3 in ccRCC are shown. (F-L) Differential expression of ACSL3 in ccRCC with (F) individual cancer stages (n = 603), (G) patient's race (n = 598), (H) patient's gender (n = 605), (I) patient's age (n = 605), (J) individual cancer grade (n = 597), (K) histological subtypes (n = 452), and (L) nodal metastasis status (n = 328). *ns*, no statistical significance; $^{*}P < 0.05$; $^{**}P < 0.01$; $^{***}P < 0.001$; $^{****}P < 0.0001$.

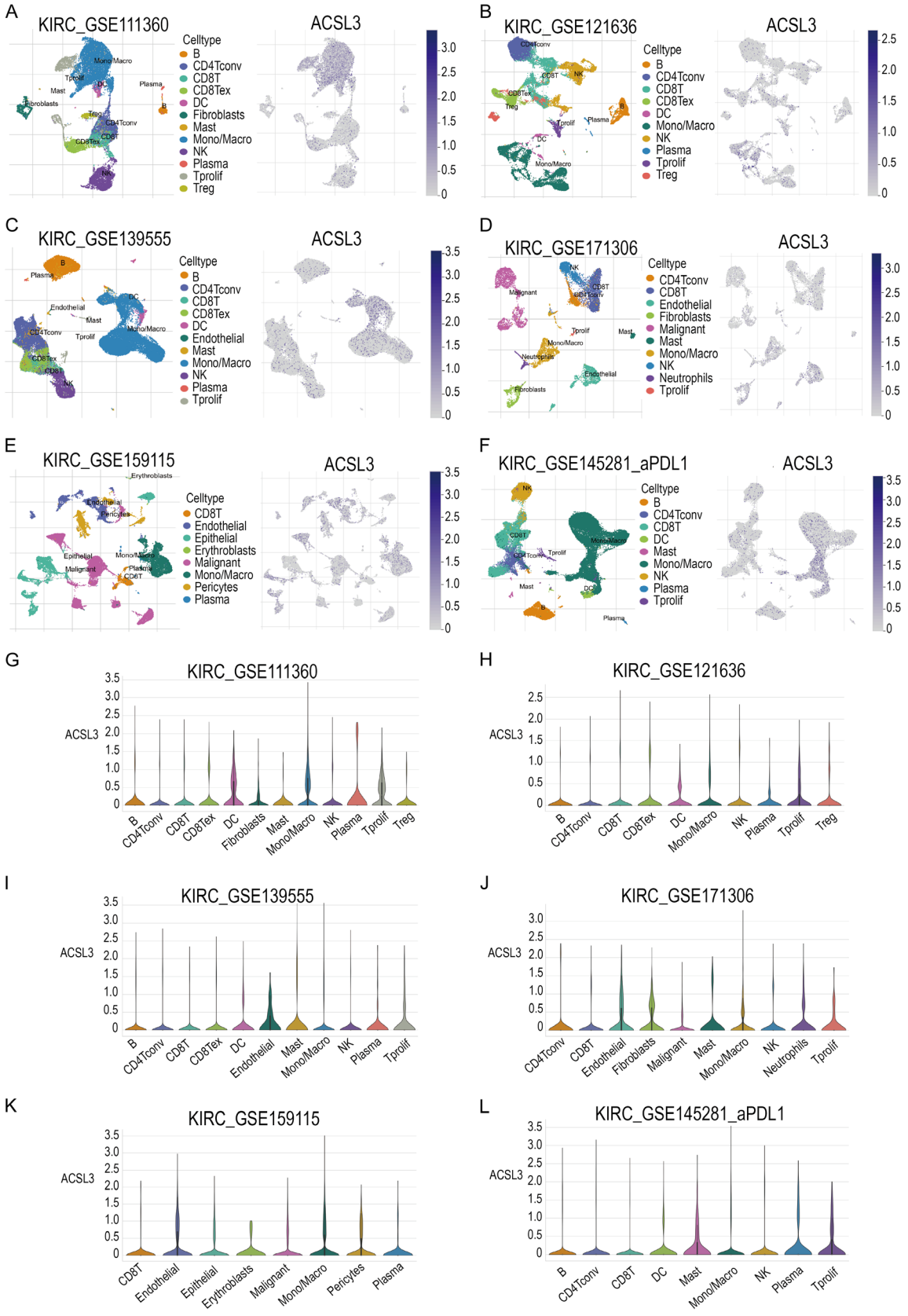
A
KIRC_GSE111360
ACSL3
Celltype
B
CD4Tconv
CD8T
CD8Tex
DC
Fibroblasts
Mast
Mono/Macro
NK
Plasma
Tprolif
Treg
B
KIRC_GSE121636
ACSL3
C
KIRC_GSE139555
ACSL3
D
KIRC_GSE171306
ACSL3
E
KIRC_GSE159115
ACSL3
F
KIRC_GSE145281_aPDL1
ACSL3
G
KIRC_GSE111360
ACSL3
H
KIRC_GSE121636
ACSL3
I
KIRC_GSE139555
ACSL3
J
KIRC_GSE171306
ACSL3
K
KIRC_GSE159115
ACSL3
L
KIRC_GSE145281_aPDL1
ACSL3

**Figure 4.** Correlation between single-cell localization and immune abundance of ACSL3 in KIRC single-cell data. (A-F) The heatmap showed the relatively high expression of ACSL3 in different cell types, such as CD4+ T cells, CD8+ T cells, monocytes, macrophages, and NK cells across the six scRNA-seq datasets, namely, (A) GSE111360, (B) GSE121636, (C) GSE139555, (D) GSE171306, (E) GSE159115, and (F) GSE145281_aPDL1. (G-L) Colocalization of ACSL3 expression in different immune cells in KIRC single-cell data. (G) GSE111360, (H) GSE121636, (I) GSE139555, (J) GSE171306, (K) GSE159115, (L) GSE145281_aPDL1.

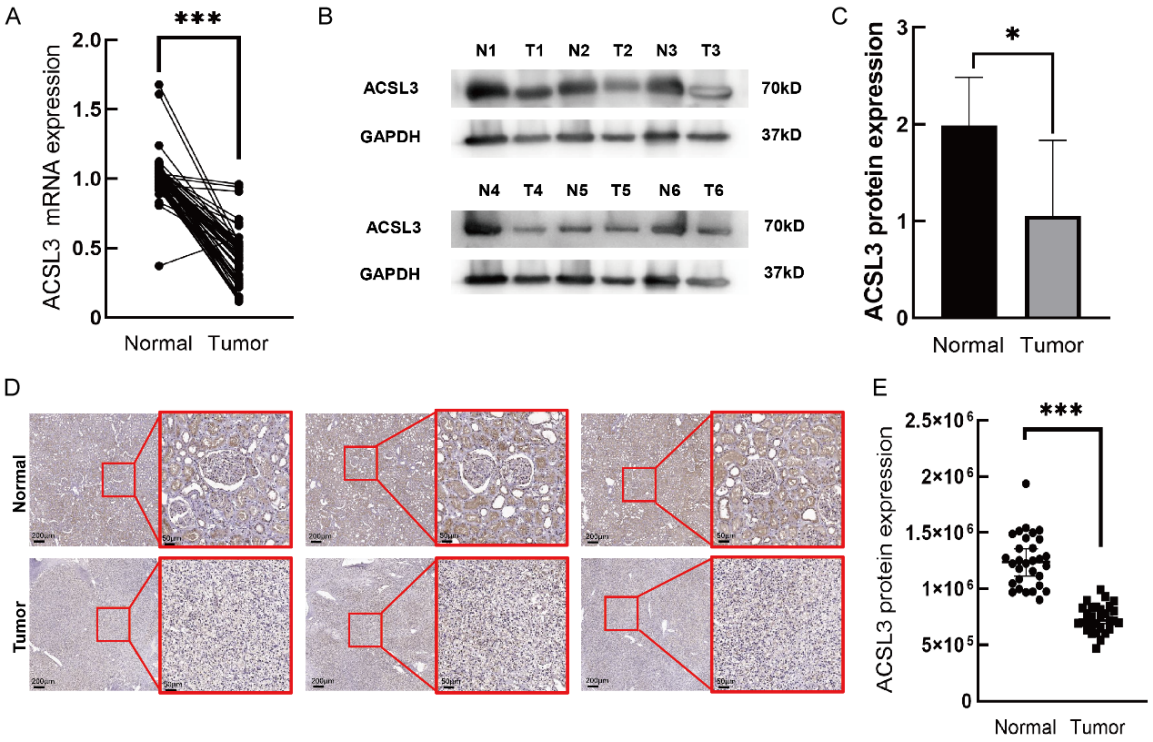


**Figure 5.** Differential mRNA expression and protein expression of ACSL3 in human primary ccRCC tissues. A. The mRNA expression levels of ACSL3 in 60 pairs of ccRCC tissues and adjacent normal renal tissues were evaluated using RT-qPCR. B, C. Western blot analysis of ACSL3 protein expression in ccRCC tissues and adjacent normal tissues. D. Representative IHC analysis of ACSL3 in ccRCC and normal renal tissue. E. Quantitative analysis of ACSL3 expression in 30 pairs of ccRCC tissues based on the mean density of IHC staining. GAPDH was used as an internal control. Error bars represent M ± SD of triplicate experiments. ns, *no* statistical significance; $^{*}P < 0.05$; $^{**}P < 0.01$; $^{***}P < 0.001$; $^{****}P < 0.0001$.

in the h-ACSL3 group than that in the control group ($P < 0.05$) (**Figure 6C**, **6D**). The results of CCK-8 analysis indicated that at 96 h, the cell proliferation rate of the h-ACSL3 group was significantly lower than that of the control group ($P < 0.05$) (**Figure 6E**). Meanwhile, the clone formation assay revealed that the number of cell colonies in the h-ACSL3 group was significantly less than that in the control group ($P < 0.05$) (**Figure 6F**).

*ACSL3 overexpression inhibits migration and invasion*

The scratch experiments demonstrated that the scratch healing rate in the h-ACSL3 group was significantly lower than that in the control group, suggesting that the migration ability of cells was significantly weakened after ACSL3 overexpression ($P < 0.05$) (**Figure 7A**, **7B**). Similar results were observed in the Transwell migration and invasion experiments, which revealed that the h-ACSL3 group had fewer cells passing through the Matrigel than the control group. The overexpression of ACSL3 significantly inhibited the migration and invasion of cells ($P < 0.05$) (**Figure 7C-E**).

*ACSL3 overexpression accelerates ccRCC cell apoptosis*

Next, we investigated the effect of ACSL3 on apoptosis by flow cytometry using the FITC/PI kit. The results FITC-/PI-, FITC+/PI-, FITC+/PI+,

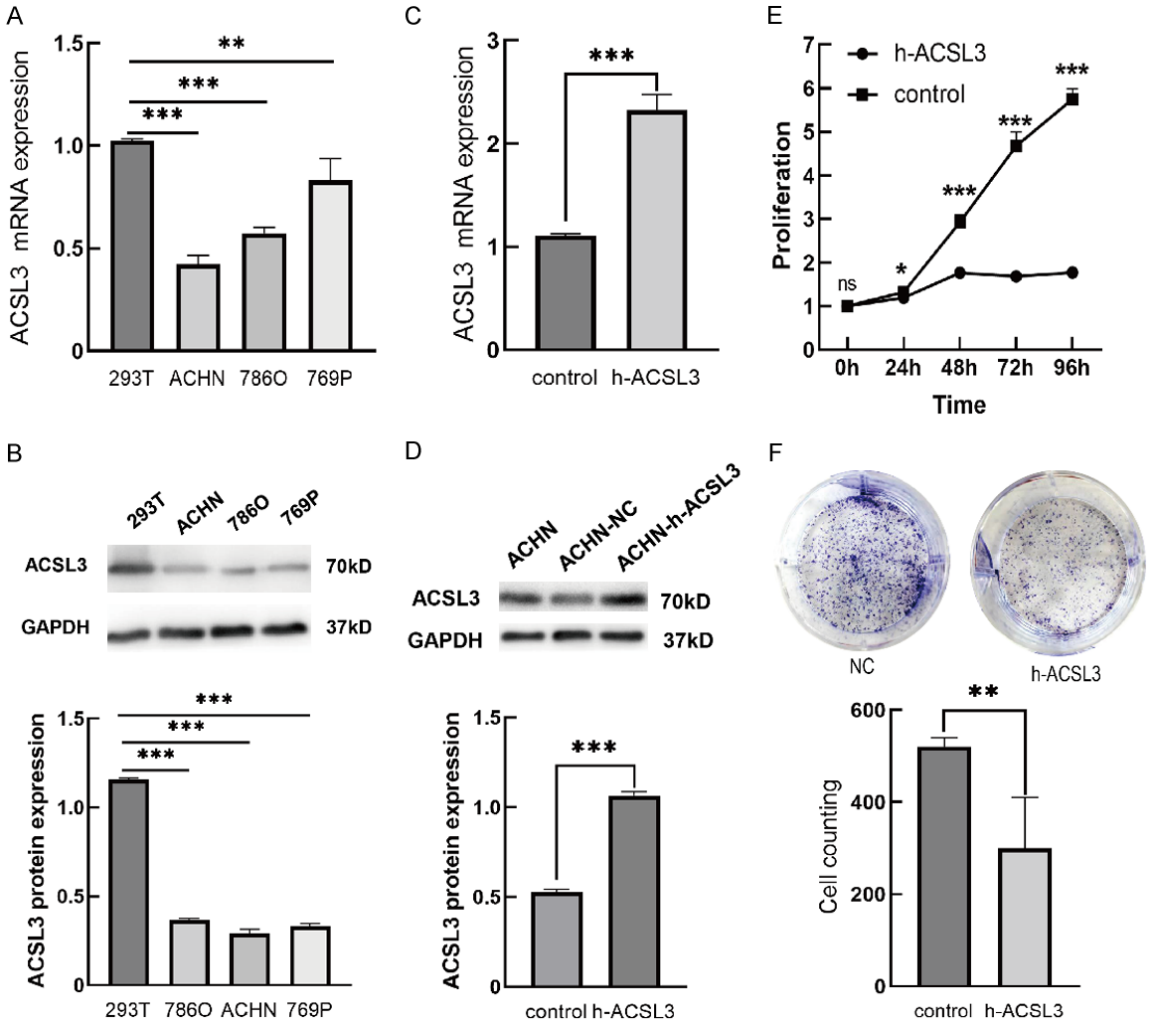


**Figure 6.** Differential expression of ACSL3 in cell lines and its effect on cell proliferation. A. RT-qPCR analysis of ACSL3 mRNA expression in ccRCC cell lines (ACHN, 769P, and 786O) and the normal renal cell line (293T). B. Western blot analysis of ACSL3 protein expression in ccRCC cell lines and the normal renal cell line. C. RT-qPCR analysis of ACSL3 mRNA expression in h-ACSL3 cells and control cells after transfection. D. Western blot analysis of the ACSL3 protein expression levels in h-ACSL3 cells and control cells after transfection. GAPDH was used as an internal control. Error bars represent M ± SD of triplicate experiments. E. CCK-8 assays were performed to detect the cell proliferation rates of h-ACSL3 cells and control cells at 0, 24, 48, 72, and 96 h. F. Clone formation ability and statistical analysis of h-ACSL3 cells and control cells. Error bars represent M ± SD of triplicate experiments. *ns*, no statistical significance; $^{*}P < 0.05$; $^{**}P < 0.01$; $^{***}P < 0.001$; $^{****}P < 0.0001$.

and FITC-/PI+ represented viable cells, early-apoptotic cells, late-apoptotic cells, and necrotic cells, respectively. The results showed that the overexpression of ACSL3 significantly increased the apoptotic rate of cells compared with the control groups ($P < 0.05$, **Figure 8A**, **8B**).

*ACSL3 overexpression inhibits lipid droplet accumulation*

Next, we performed the Oil Red O staining. Through microscopic analysis, we observed that the lipid droplet content of cells in the h-ACSL3 group after Oil Red O staining was significantly reduced compared than that in the control group (**Figure 8C**). These results suggested that ACSL3 might play an important role in the abnormal accumulation of lipid droplets in ccRCC. ACSL3 might regulate the lipid droplet formation and abnormal aggregation.

## Discussion

Cancer, with its complex pathogenesis and high mortality rate, is an important disease that

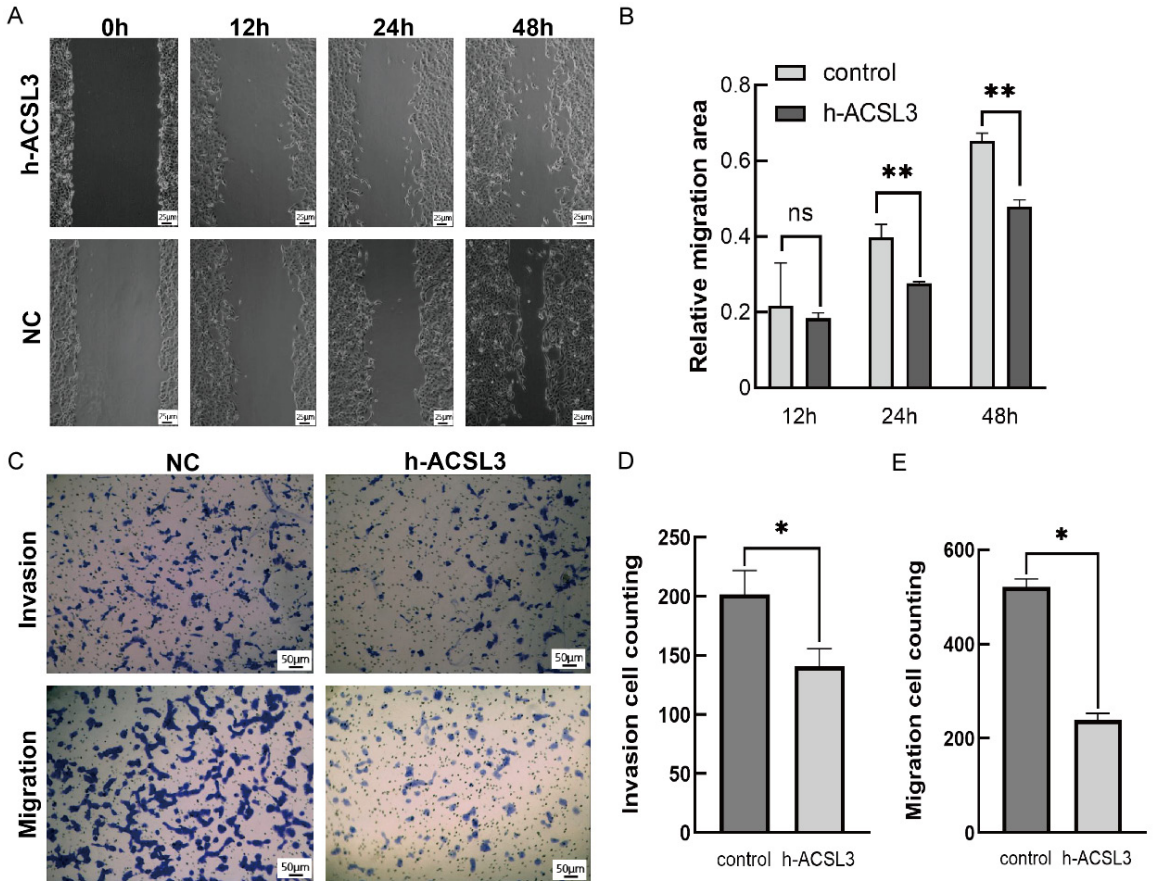


**Figure 7.** Effect of ACSL3 on the migration and invasion of ccRCC cells. A. The scratch test was used to determine the migration ability of the h-ACSL3 cells and control cells at 0,12, 24, and 48 h. B. The healing rate of the scratch test was analyzed. C. The invasion and migration abilities of h-ACSL3 cells and control cells were detected using Transwell assay. D. Statistical analysis of the number of h-ACSL3 cells and control cells based on the Transwell invasion assay. E. Statistical analysis of the number of h-ACSL3 cells and control cells based on the Transwell migration assay. Error bars represent M ± SD of triplicate experiments. *ns*, no statistical significance; $^{*}P < 0.05$; $^{**}P < 0.01$; $^{***}P < 0.001$; $^{****}P < 0.0001$.

affects human life and health and is a major cause of human death globally. Understanding the risk factors for cancer development, early detection, and effective treatment are prerequisites for improving overall patient survival and prognosis. Previous studies have shown that lipid metabolism is disrupted in tumors, and cancer cells reprogram metabolic pathways to meet cell growth needs. The incidence and mortality rates of renal cancer (RCC) are increasing every year [4]. ccRCC accounts for about 75%-80% of all RCC types and is characterized by high mortality and poor prognosis [23]. Thus, the early diagnosis and treatment of ccRCC are critical to reducing patient mortality. ccRCC is a metabolic disease characterized by abnormal lipid metabolism, which is evidenced by the massive lipid accumulation in tubular cells [6, 24, 25]. Studies have shown that fatty acid oxidation (FAO) is reduced, and enzymes involved in fat storage are increased in ccRCC tissues compared to normal renal tissues [7-9]. An abnormal accumulation of cholesteryl esters and long-chain fatty acids is observed in ccRCC tissues [26, 27], which provides nutritional raw materials for the proliferation and metastasis of tumor cells. However, the mechanisms by which disorders of fatty acid metabolism occur in ccRCC have not yet been investigated, and therefore the development of novel tumor markers could help in the diagnosis and treatment of ccRCC.

ACSL3 can activate palmitic acid, catalyze the synthesis of fatty acyl-CoA esters [13], and play an important role in the fatty acid metabolism

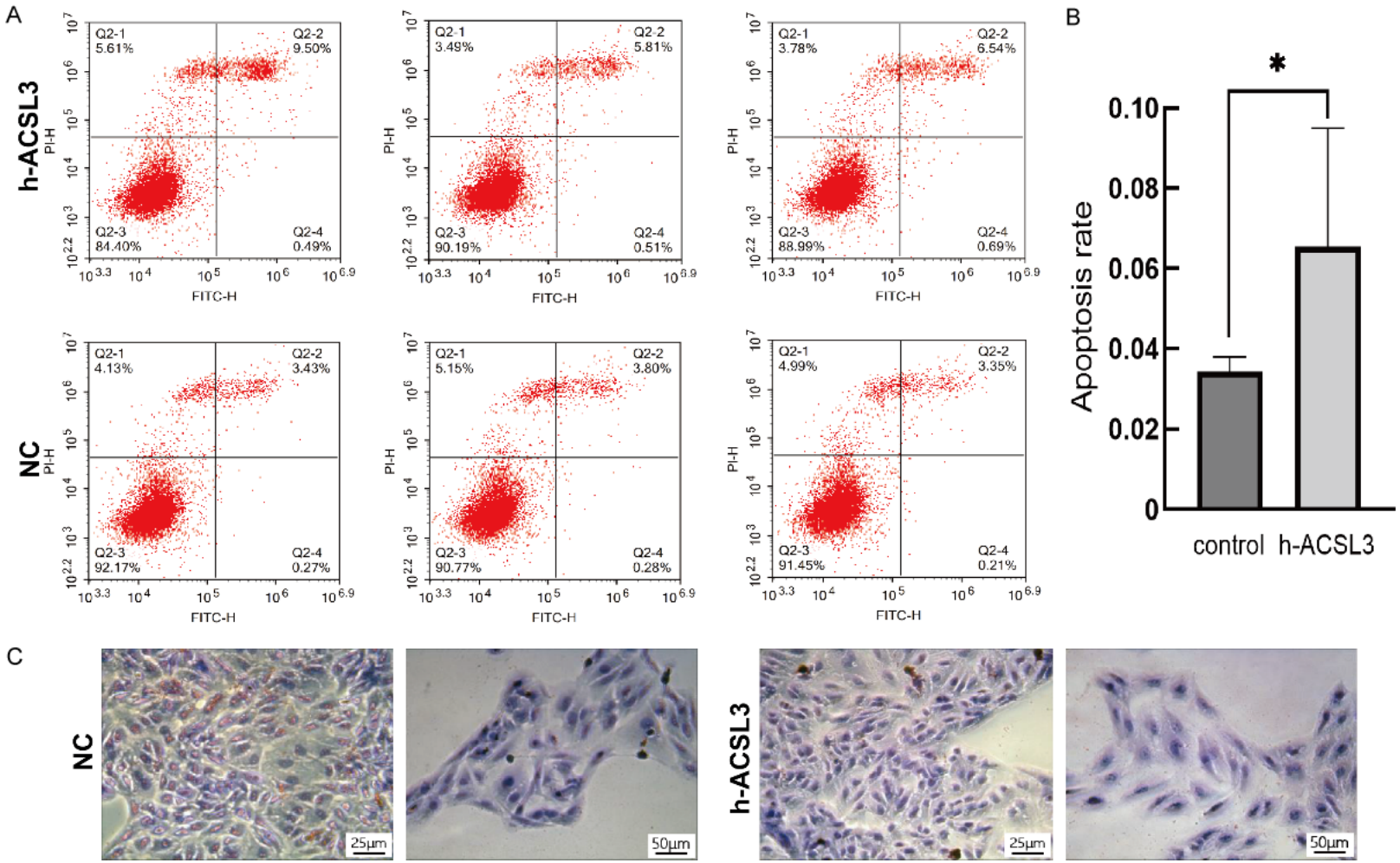


**Figure 8.** Effect of ACSL3 on the apoptosis and lipid accumulation of ccRCC cells. A. Annexin V assays followed by flow cytometry were used to evaluate the apoptosis rate of h-ACSL3 cells and control cells. B. Statistical analysis of the results of flow apoptosis experiments in h-ACSL3 cells and control cells. C. Oil red O staining of h-ACSL3 cells and control cells. Error bars represent M ± SD of triplicate experiments. *ns*, no statistical significance; $^{*}P < 0.05$; $^{**}P < 0.01$; $^{***}P < 0.001$; $^{****}P < 0.0001$.

of cells [28]. Previous studies have shown that abnormal ACSL3 expression plays an important role in the development and progression of various tumors [15, 16]. For example, ACSL3 overexpression was closely associated with NSCLC, prostate cancer, human fibrosarcoma, leiomyosarcoma, rhabdomyosarcoma, breast cancer, melanoma, and pancreatic cancer [19-22]. However, the expression pattern, prognostic value, and biological significance of ACSL3 in ccRCC are still unclear. In this study, we explored the effect of ACSL3 on the biological functions of ccRCC cells for the first time. The bioinformatics analysis revealed that ACSL3 was downregulated in ccRCC and that the prognosis of patients with lower ACSL3 expression was poor, indicating that ACSL3 may be a potential oncogene in the development of ccRCC.

Through GO and KEGG pathway functional enrichment analysis, we found that ACSL3 was mainly closely associated with lipid catabolism, lipid biosynthesis, and PPAR signaling pathways. It has been previously shown that lipid metabolism disorders exist in tumors and that cancer cells meet their needs for energy expenditure, stress tolerance, proliferation, and microenvironment alterations by reprogramming metabolic pathways [5]. The N-terminal domain of ACSL3 is responsible for regulating lipid droplet location and fatty acid uptake, which can help ACSL3 participate in the in vivo metabolism of fatty acids [29]. These results indicated that ACSL3 was associated with fatty acid metabolism disorders in tumors.

The tumor immune microenvironment plays an important role in tumor development and prognosis, immune escape, and immunotherapy, while immune cells can promote or inhibit tumor growth and metastasis. We analyzed the changes in the abundance of immune cells at a single-cell level in ccRCC and observed that ACSL3 was predominantly associated with the localization and distribution of mononuclear macrophages (mono/macro), CD8 T cells, mast cells, and NK cells in five single-cell datasets from primary tumors. In another dataset of metastatic tumors treated using immunotherapy, we observed that ACSL3 was correlated with the distribution of mast cells, CD4T conv cells, NK cells, and B cells. CD8+ T cells, macrophages, dendritic cells (DCs), and other immune cells are closely related to the occurrence and development of tumors and may mediate the occurrence of tumors [30]. Immunotherapy has gradually emerged in recent years, and some patients have achieved better prognoses using immunotherapy, whereas others have a poorer prognosis, which may be closely related to the TME and the level of immune cell infiltration [31]. There is a complex relationship between the immune microenvironment and tumor cells, and we hypothesize that ACSL3 expression can promote the relationship between them.Thus, the above results will help identify new indicators or adjuvant therapeutic targets to monitor the effectiveness of immunotherapy.

Abnormal gene expression is a common feature of cancer cells and is closely related to abnormal cell growth, tumor occurrence, and development. We analyzed the correlation between the type of mutations in ACSL3 in ccRCC and clinicopathological factors. The results indicated that the mutation types of ACSL3 in ccRCC were mainly “mutation” and “amplification”. Moreover, ACSL3 was significantly correlated with the grade, stage, age, nodal metastasis status, subtype, gender, and race of ccRCC patients.

In this study, we demonstrated that ACSL3 was closely associated with the expression, prognosis, pathological factors, and tumor immunity in ccRCC. To our knowledge, this study is the first to experimentally verify the functional impact of ACSL3 on ccRCC. We first demonstrated that ACSL3 was downregulated in ccRCC clinical tissue samples and cell lines. Then, we performed transfections in the ACHN cells. After overexpression of the ACSL3 gene, the proliferation, migration, and invasion of ccRCC cells were significantly inhibited, the apoptotic ability was significantly increased. The GO and KEGG enrichment analysis indicated that ACSL3 mainly affected lipid synthesis and lipid metabolism in cells. And previous studies have demonstrated that ACSL3 was an important enzyme in the fatty acid metabolic pathway, while an increasing number of recent studies have confirmed the presence of lipid metabolism disorders in ccRCC. Therefore, we explored the potential effects of ACSL3 overexpression on lipid droplet aggregation in ccRCC. The Oil Red O staining shown that the accumulation of lipid

droplets in the h-ACSL3 group was significantly reduced than that in control group. These results proved that ACSL3 gene may be associated with the occurrence, development, metastasis, and lipid droplet accumulation of ccRCC. Therefore, ACSL3 could be a potential therapeutic target for inhibiting disorders of lipid metabolism, which could help develop clinical drugs. The development of ACSL3 inhibitors is currently in the preliminary stage and requires further in-depth study.

Although the diagnosis, surgical treatment, radiation therapy, and molecular therapy of ccRCC are advancing with the development of medical technology, which can enable patients with ccRCC to have a longer survival time, the 5-year survival rate for patients with ccRCC remains low. Early detection of ccRCC is critical to reducing patient mortality, which makes the development of early diagnostic biomarkers vital. In this study, we explored the expression and biological function of ACSL3 in ccRCC and it was observed that ACSL3 might be a key factor in the progression of ccRCC which is a foundation for research on the clinical diagnosis and treatment of ccRCC.

## Conclusion

In conclusion, we recognized that ACSL3 expression was significantly downregulated in ccRCC and was associated with clinicopathological factors, poor prognosis, and immune microenvironment. We demonstrated for the first time that ACSL3 overexpression inhibits the proliferation, migration, invasive ability, and lipid droplet accumulation of ccRCC cells and promotes the apoptosis of ccRCC cells. Thus, ACSL3 might represent a novel biomarker for the treatment of ccRCC.

## Acknowledgements

This work was supported by grants from the National Natural Science Foundation of China (No. 81970662); Beijing Bethune Charitable Foundation, Special Research Fund for Urological Oncology (No. mnzl202029); Scientific Research Funding Project of Returned Overseas Scholars of Shanxi Province (No. 2021-160); Applied Basic Research Project of Shanxi Province (No. 20210302123242).

## Disclosure of conflict of interest

The authors declare that the research was conducted in the absence of any commercial or financial relationships that could be construed as a potential conflict of interest.

**Address correspondence to:** Dr. Dongwen Wang, Department of Urology, National Cancer Center/National Clinical Research Center for Cancer/Cancer Hospital & Shenzhen Hospital, Chinese Academy of Medical Sciences and Peking Union Medical College, No. 113, Baohe Avenue, Longgang District, Shenzhen 518116, Guangdong, P. R. China. E-mail: urology2007@126.com

## References

[1] Xia C, Dong X, Li H, Cao M, Sun D, He S, Yang F, Yan X, Zhang S, Li N and Chen W. Cancer statistics in China and United States, 2022: profiles, trends, and determinants. Chin Med J (Engl) 2022; 135: 584-590.

[2] Lai Y, Tang F, Huang Y, He C, Chen C, Zhao J, Wu W and He Z. The tumour microenvironment and metabolism in renal cell carcinoma targeted or immune therapy. J Cell Physiol 2021; 236: 1616-1627.

[3] Bukavina L, Bensalah K, Bray F, Carlo M, Challacombe B, Karam JA, Kassouf W, Mitchell T, Montironi R, O'Brien T, Panebianco V, Scelo G, Shuch B, van Poppel H, Blosser CD and Psutka SP. Epidemiology of renal cell carcinoma: 2022 update. Eur Urol 2022; 82: 529-542.

[4] Sung H, Ferlay J, Siegel RL, Laversanne M, Soerjomataram I, Jemal A and Bray F. Global cancer statistics 2020: GLOBOCAN estimates of incidence and mortality worldwide for 36 cancers in 185 countries. CA Cancer J Clin 2021; 71: 209-249.

[5] Sun L, Zhang H and Gao P. Metabolic reprogramming and epigenetic modifications on the path to cancer. Protein Cell 2022; 13: 877-919.

[6] Courtney KD, Bezwada D, Mashimo T, Pichumani K, Vemireddy V, Funk AM, Wimberly J, McNeil SS, Kapur P, Lotan Y, Margulis V, Cadeddu JA, Pedrosa I, DeBerardinis RJ, Malloy CR, Bachoo RM and Maher EA. Isotope tracing of human clear cell renal cell carcinomas demonstrates suppressed glucose oxidation in vivo. Cell Metab 2018; 28: 793-800, e792.

[7] Wettersten HI, Hakimi AA, Morin D, Bianchi C, Johnstone ME, Donohoe DR, Trott JF, Aboud OA, Stirdivant S, Neri B, Wolfert R, Stewart B, Perego R, Hsieh JJ and Weiss RH. Grade-dependent metabolic reprogramming in kidney cancer revealed by combined proteomics and metabolomics analysis. Cancer Res 2015; 75: 2541-2552.

[8] Horiguchi A, Asano T, Asano T, Ito K, Sumitomo M and Hayakawa M. Fatty acid synthase over expression is an indicator of tumor aggressiveness and poor prognosis in renal cell carcinoma. J Urol 2008; 180: 1137-1140.

[9] von Roemeling CA, Marlow LA, Wei JJ, Cooper SJ, Caulfield TR, Wu K, Tan WW, Tun HW and Copland JA. Stearoyl-CoA desaturase 1 is a novel molecular therapeutic target for clear cell renal cell carcinoma. Clin Cancer Res 2013; 19: 2368-2380.
[10] Cheng C, Geng F, Cheng X and Guo D. Lipid metabolism reprogramming and its potential targets in cancer. Cancer Commun (Lond) 2018; 38: 27.
[11] Wu Z, Sun J, Liao Z, Qiao J, Chen C, Ling C and Wang H. An update on the therapeutic implications of long-chain acyl-coenzyme a synthetases in nervous system diseases. Front Neurosci 2022; 16: 1030512.
[12] Soupene E and Kuypers FA. Mammalian long-chain acyl-CoA synthetases. Exp Biol Med (Maywood) 2008; 233: 507-521.
[13] Quan J, Bode AM and Luo X. ACSL family: the regulatory mechanisms and therapeutic implications in cancer. Eur J Pharmacol 2021; 909: 174397.
[14] Kassan A, Herms A, Fernandez-Vidal A, Bosch M, Schieber NL, Reddy BJ, Fajardo A, Gelabert-Baldrich M, Tebar F, Enrich C, Gross SP, Parton RG and Pol A. Acyl-CoA synthetase 3 promotes lipid droplet biogenesis in ER microdomains. J Cell Biol 2013; 203: 985-1001.
[15] Tang Y, Zhou J, Hooi SC, Jiang YM and Lu GD. Fatty acid activation in carcinogenesis and cancer development: essential roles of long-chain acyl-CoA synthetases. Oncol Lett 2018; 16: 1390-1396.
[16] Fernandez LP, Merino M, Colmenarejo G, Moreno-Rubio J, Sanchez-Martinez R, Quijada-Freire A, Gomez de Cedron M, Reglero G, Casado E, Sereno M and Ramirez de Molina A. Metabolic enzyme ACSL3 is a prognostic biomarker and correlates with anticancer effectiveness of statins in non-small cell lung cancer. Mol Oncol 2020; 14: 3135-3152.
[17] Saliakoura M, Reynoso-Moreno I, Pozzato C, Rossi Sebastiano M, Galie M, Gertsch J and Konstantinidou G. The ACSL3-LPIAT1 signaling drives prostaglandin synthesis in non-small cell lung cancer. Oncogene 2020; 39: 2948-2960.
[18] Migita T, Takayama KI, Urano T, Obinata D, Ikeda K, Soga T, Takahashi S and Inoue S. ACSL3 promotes intratumoral steroidogenesis in prostate cancer cells. Cancer Sci 2017; 108: 2011-2021.
[19] Radif Y, Ndiaye H, Kalantzi V, Jacobs R, Hall A, Minogue S and Waugh MG. The endogenous subcellular localisations of the long chain fatty acid-activating enzymes ACSL3 and ACSL4 in sarcoma and breast cancer cells. Mol Cell Biochem 2018; 448: 275-286.
[20] Wright HJ, Hou J, Xu B, Cortez M, Potma EO, Tromberg BJ and Razorenova OV. CDCP1 drives triple-negative breast cancer metastasis through reduction of lipid-droplet abundance and stimulation of fatty acid oxidation. Proc Natl Acad Sci U S A 2017; 114: E6556-E6565.
[21] Ubellacker JM, Tasdogan A, Ramesh V, Shen B, Mitchell EC, Martin-Sandoval MS, Gu Z, McCormick ML, Durham AB, Spitz DR, Zhao Z, Mathews TP and Morrison SJ. Lymph protects metastasizing melanoma cells from ferroptosis. Nature 2020; 585: 113-118.
[22] Rossi Sebastiano M, Pozzato C, Saliakoura M, Yang Z, Peng RW, Galie M, Oberson K, Simon HU, Karamitopoulou E and Konstantinidou G. ACSL3-PAI-1 signaling axis mediates tumor-stroma cross-talk promoting pancreatic cancer progression. Sci Adv 2020; 6: eabb9200.
[23] Padala SA and Kallam A. Clear cell renal carcinoma. StatPearls: Treasure Island (FL); 2022.
[24] Fritz V, Benfodda Z, Rodier G, Henriquet C, Iborra F, Avances C, Allory Y, de la Taille A, Culine S, Blancou H, Cristol JP, Michel F, Sardet C and Fajas L. Abrogation of de novo lipogenesis by stearoyl-CoA desaturase 1 inhibition interferes with oncogenic signaling and blocks prostate cancer progression in mice. Mol Cancer Ther 2010; 9: 1740-1754.
[25] Huang WC, Li X, Liu J, Lin J and Chung LW. Activation of androgen receptor, lipogenesis, and oxidative stress converged by SREBP-1 is responsible for regulating growth and progression of prostate cancer cells. Mol Cancer Res 2012; 10: 133-142.
[26] Hakimi AA, Reznik E, Lee CH, Creighton CJ, Brannon AR, Luna A, Aksoy BA, Liu EM, Shen R, Lee W, Chen Y, Stirdivant SM, Russo P, Chen YB, Tickoo SK, Reuter VE, Cheng EH, Sander C and Hsieh JJ. An integrated metabolic atlas of clear cell renal cell carcinoma. Cancer Cell 2016; 29: 104-116.
[27] Gebhard RL, Clayman RV, Prigge WF, Figenshau R, Staley NA, Reesey C and Bear A. Abnormal cholesterol metabolism in renal clear cell carcinoma. J Lipid Res 1987; 28: 1177-1184.
[28] Kimura H, Arasaki K, Ohsaki Y, Fujimoto T, Ohtomo T, Yamada J and Tagaya M. Syntaxin 17 promotes lipid droplet formation by regulating the distribution of acyl-CoA synthetase 3. J Lipid Res 2018; 59: 805-819.
[29] Rossi Sebastiano M and Konstantinidou G. Targeting long chain acyl-coa synthetases for cancer therapy. Int J Mol Sci 2019; 20: 3624.
[30] Greten FR and Grivennikov SI. Inflammation and cancer: triggers, mechanisms, and consequences. Immunity 2019; 51: 27-41.
[31] Chen VE, Greenberger BA, Taylor JM, Edelman MJ and Lu B. The underappreciated role of the humoral immune system and B cells in tumorigenesis and cancer therapeutics: a review. Int J Radiat Oncol Biol Phys 2020; 108: 38-45.